Flow Structure Detection with Smoothed Particle Hydrodynamics

B. Tóth and K. G. Szabó
Department of Hydraulic and Water Resources Engineering
BME Budapest University of Technology and Economics
Budapest, Hungary
toth.balazs@epito.bme.hu and szabo@vit.bme.hu

***Abstract*—We discuss how existing flow structure detection methods can be realised in Smoothed Particle Hydrodynamcs (SPH) simulations. We demonstrate the use of the Δ criterion for the detection of instantaneous Eulerian flow structures. The standard calculation of the velocity gradient tensor (VGT) results too noisy gradient field. We propose a correction method based on the idea of XSPH that yields a much smoother VGT field, enabling significantly more accurate structure detection. We also demonstrate on test cases the process in which the instantaneous Eulerian tools are used to locate Lagrangian coherent flow structures.**

I. Introduction

Finding reliable algorithms to pinpoint a flow structure in the data of a sizable computer simulation has become a key issue in most fields of computational fluid dynamics. The different flow structure identification methods can be roughly classified as Eulerian or Lagrangian.

Eulerian methods operate on the instantaneous flow field and treat it as if it was steady. This is a serious drawback with respect to Lagrangian ones that try to capture the flow features evolving in time. However, the computational demands on resources have so far prevented the latter ones from becoming routine analytic tasks. The best approach seems to be the application of an appropriate Eulerian criterion at some time to the instantaneous fields to capture *candidates* of Lagrangian flow structures. Having narrowed down to a much smaller part of the fluid, high demand calculations can be started to further verify or exclude the existence of Lagrangian flow features.

An important goal of the Eulerian methods is to detect vortices, and, therefore, a great number of methods have been developed for that purpose. Unfortunately, the very meaning of a vortex is unclear: high vorticity and circular motion, the main characteristics of a vortex, do not necessarily coincide, like e.g. in shear layers. It seems that as many definitions of vortex exist as many vortex detection algorithms. Instead of seeking for a good definition of a vortex, one may look for a good vortex detection algorithm instead. Apart from practical issues three principal requirements have been formulated: a good algorithm has to be dimensionless [1], frame-independent [2] and capable of describing compressible fluids [3].

The last point seems to be the most decisive from the point of SPH, which is, by design, compressible — at least weakly. Therefore in Section II, following the recommendations of [3], we present the concept of the Δ-criterion (which also happens to be Galilean invariant) for two and three dimensional SPH applications. Another key issue is whether it is possible to achieve such a precision in SPH that the spatial derivatives of the velocity field necessary for the Eulerian criteria can be calculated: this problem will be discussed in Section III.

Finally, in Section IV, we shall turn to the investigation of Lagrangian flow structures. As SPH is a genuine Lagrangian method, the field variables are related to particles in the material frame. This makes SPH a very promising potential tool for Lagrangian structure detection problems. The central notion in the Lagrangian problems is *mixing*: certain types of Lagrangian coherent structures are defined as the ones that maintain their identity, other types correspond to barriers to material transport. We calculate two quantities that characterize the local strength of mixing in suspected Lagrangian coherent structures: relative dispersion and finite time Lyapunov exponents (FTLE).

The computations we present have been carried out by our parallel SPH solver written in CUDA and C++.

II. Theoretical Background

A. Flow Structures and Dynamical Systems

The flow pattern of *steady flows* can be completely described by the local analysis of their stagnation points and the global analysis of their invariant manifolds [4]. Due to the achievements of dynamical systems' theory this seems to be a closed problem, even if in specific cases the actual computations can be challenging.

The simplest case is that of isochoric (divergence free) steady plane flows; their most typical flow features are

- two types of stagnation points — elliptic (centres) and hyperbolic (saddles) points —,
- elliptic islands containing closed streamlines, which loop around the centres, and
- separatrices — stable and unstable invariant manifolds of the saddles — that form boundaries among the elliptic islands and regions of unbounded flow.

It is natural to identify elliptic islands with vortices and elliptic stagnation points with vortex centres. There is an immediate relation between these (in fact Eulerian) flow structures to the

Lagrangian view of the flow. Since fluid particles following streamlines cannot cross separtrices they act as *transport barriers*: passive tracers that follow the streamlines of the flow get trapped within the elliptic islands thus showing only a limited dispersion.

Steady flows in three dimensions and of compressible fluids allow more types for stagnation points and more complex topology but the previous picture prevails. Further generalization from steady to strictly time periodic flows is also possible by extending the phase space to a fourth dimension. Even if adding small perturbations to such systems, the above mental picture of flow features remains valid up to a certain extent. Certain transport barriers can survive small perturbation (KAM tori) thus maintaining particle traps, others become permeable (Can-tori) but still act as obstacles allowing only slow leakage. [4]

As the perturbations become substantial, both the spatial extent and the lifetime of the elliptic islands become diminished.

In general unsteady flows of real fluids a plethora of flow structures exist, e.g. Zabusky has collected dozens of interacting fluid dynamical coherent structures in his glossary in [5]. In turbulence coherent structures transport concentrated energy (and enstrophy) packages between the macroscopic and dissipative scales [6]. In geophysical and environmental fluid dynamical problems the transport of advected pollutants and nutrients by coherent flow structures effect the development of life conditions [7]. These and several other important scientific and engineering problems require robust, computationally feasible algorithms for the identification of coherent structures often from very large data sets. Even though these practical problems are not tractable by the elegant mathematical way described above, the mental concepts have fertilized the development of flow structure detection algorithms.

B. Eulerian Flow Structure Criteria

Many Eulerian methods are limited to the local stability analysis of the instantaneous VGT[1]

$$A^{ij} = \frac{\partial v^i}{\partial x^j}\,, \tag{1}$$

which is in general an asymmetric matrix. It can be decomposed as

$$A^{ij} = S^{ij} + W^{ij}\,, \tag{2}$$

to a symmetric and a skew-symmetric part

$$S^{ij} = (A^{ij} + A^{ji})/2$$
$$W^{ij} = (A^{ij} - A^{ji})/2\,,$$

which are referred as strain (S^{ij}) and rotation or swirl (W^{ij}) tensors, the latter just expressing the vorticity in tensorial form.

[1]Throughout this paper we use superscripts to index spatial coordinates and subscripts to index SPH particles. We restrict our discussion to Cartesian coordinates, therefore no distinction between contravariant and covariant coordinates are necessary. We follow the convention that double appearance of a superscript symbol in a term implies summation over that symbol.

The characteristic equation for the eigenvalues (λ) of A^{ij} in two and three dimensions are

$$\lambda^2 + P\lambda + Q_{2D} = 0, \tag{3}$$

and

$$\lambda^3 + P\lambda^2 + Q\lambda + R = 0, \tag{4}$$

respectively, where the P, Q and R coefficients are the first, second and third scalar invariants of the VGT.[2] For divergence free flows the first invariant vanishes,

$$P = -A^{ii} = -\nabla v = 0\,, \tag{5}$$

which restricts the sum of all eigenvalues to zero.

a) Incompressible case: In two dimensional flows of incompressible fluids (5) implies that the eigenvalues of the VGT form either a pair of pure imaginary numbers or a pair of real numbers with opposite signs depending on the sign of the second scalar invariant. Weiss [8] introduced the terms 'elliptical' and 'hyperbolic' regions for the subdomains

$$Q_{2D} > 0 \tag{6}$$

and

$$Q_{2D} < 0\,, \tag{7}$$

respectively, that match the types of any possibly existing stagnation points within them. It seems tempting to identify vortical structures using (6), the *two dimensional Q criterion for vorticity*, and its opposite (7) to locate hyperbolic separatrices, since in steady plane flows the vortex centers are always located in the elliptical region and separatrices always emanate from a saddle within a hyperbolic region.

Unfortunately, this simple criterion is not suitable to proper identification: some parts of elliptic islands always belong to the hyperbolic subdomain; the zero isoline of Q_{2D} does not follow the shape of the elliptic islands, often crossing the separatrices; elliptic regions may occur at locations without any actual vortical motion, yielding false positive vortex detections. A typical remedy is to use a Q_{2D} threshold that differs from 0; however, when there is a wide range of vortex strength, *thresholding* causes false negative identification of weak vortices without relieving from the problem of false positive cases. Some authors tried to improve the reliability of the *purely kinematic* Q_{2D} criterion (6) by combining it with a seek for pressure minima as well, thus turning it to a *dynamical* vortex detection criterion, but this method is also fallible in case of unsteady plane flows.

Despite of its problems, the Q_{2D} criterion has gained popularity due to its straightforward applicability.

[2]The reader is warned that there is absolutely no uniformity in the literature in these notations, the coefficients and even the signs of these quantities vary. We use a notation here to emphasise the analogies between the two and three dimensional cases.

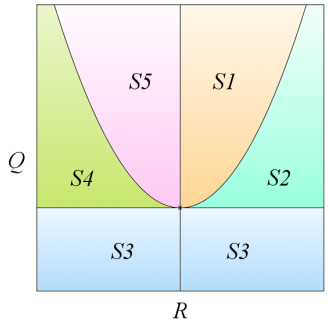

Fig. 1. Phase portrait of a compressible two dimensional flows. S1: unstable focus, S2: unstable node, S3: saddle, S4: stable node, S5: stable focus.

b) Compressible case: When the flow is not divergence free, like the flow on free surfaces, the discriminant of the quadratic characteristic equation (3) is, in general

$$\Delta_{2D} = P^2 - 4Q_{2D}. \tag{8}$$

The local stability map in the P—Q in two dimensions is shown in Fig. 1. Now the *two dimensional* Δ *criterion*

$$\Delta_{2D} > 0 \tag{9}$$

signals the region with complex pair eigenvalues and thus can be considered as an indicator of potentially rotating motion, since stagnation points here can be centres ($P = 0$), stable ($P < 0$) and unstable ($P > 0$) foci. Saddle points can exist wherever $Q_{2D} < 0$, likewise in the incompressible case before, but two other types of hyperbolicity can be present if $Q_{2D} > 0$ and $\Delta_{2D} < 0$. The relationship between the two dimensional Q_{2D} and Δ_{2D} criteria can be summarised as

$$Q_{2D} < 0 \Rightarrow \Delta_{2D} > 0,$$
$$\Delta_{2D} < 0 \Rightarrow Q_{2D} > 0.$$

It was Okubo [9] who first related the Eulerian eigenvalue spectrum of the VGT to Lagrangian behaviour. He found that diffusive dispersion of surface floater particles becomes stable around steady stagnation points falling in the quadrant

$$P < 0, Q_{2D} > 0 \tag{10}$$

indicating the presence of a *trapping region*. This criterion is necessary and sufficient. It is noteworthy that the (instantaneous) Eulerian Δ-criterion does not match the (instantaneous) Lagrangian criterion.

1) Three dimensional flows:

a) Incompressible case: For three dimensional incompressible flows the scalar invariants of the cubic characteristic equation (4) are

$$P = -A^{ii} = 0, \tag{11}$$
$$Q = -A^{im}A^{mi}/2 \equiv -\left(S^{ij}S^{ji} + W^{ij}W^{ji}\right)/2, \tag{12}$$
$$R = -A^{im}A^{mk}A^{ki}/3 \equiv -S^{ij}S^{jk}S^{ki}/3 - W^{ij}W^{jk}S^{ki}, \tag{13}$$

The corresponding discriminant of (4) is

$$\Delta = (Q/3)^3 + (R/2)^2. \tag{14}$$

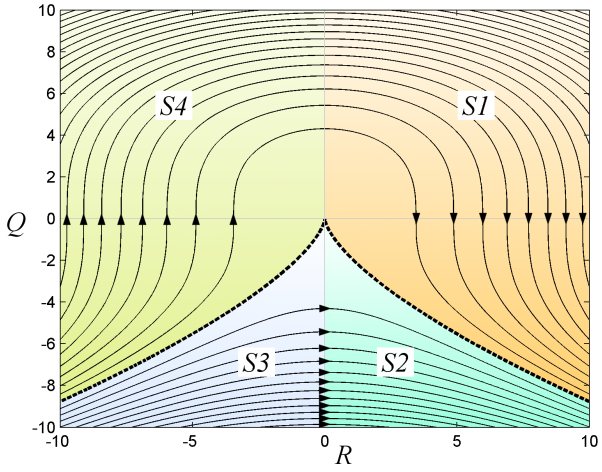

Fig. 2. The phase portrait of the VGT for incompressible three dimensional flows. The dashed line shows the zero disciminant curve. S1: compressing unstable focus. S2: node compressing in one direction, S3: node stretching in one direction, S4: stretching stable focus.

The classification of the local flow behaviour can be easily represented in the plane of the second and third invariants, Fig. 2. The $\Delta = 0$ curve separates the Q—R plane into two regions. In the region belonging to $\Delta < 0$ all three eigenvalues of the VGT are real numbers, while the $\Delta > 0$ region corresponds to one real and a pair of complex eigenvalues. [10] The Q axis subdivides both regions in such a way that the $R < 0$ half plane corresponds to local one dimensional expansion and two dimensional contraction, while this dimesionality is exchanged in the other half plane $R > 0$. The $R = 0$ case falls back to the two dimensional incompressible problem. Similarly to the two dimensional cases, one can identify the $\Delta < 0$ region with hyperbolic, strain dominated behaviour and

$$\Delta = (Q/3)^3 + (R/2)^2 > 0 \tag{15}$$

becomes the *three dimensional incompressible* Δ *vortex criterion* that identifies the rotation dominated behaviour; vortices in the left and right half planes of the Q—R plane are stretching and flattening vortices.

Similarly to the two dimensional compressible case, it is possible to use a (now three dimensional) Q criterion as well, which gives a more stringent criterion for hyperbolic behaviour and less stringent one for vortex identification:

$$Q > 0 \Rightarrow \Delta > 0, \quad \Delta < 0 \Rightarrow Q < 0. \tag{16}$$

b) Compressible case: As we relinquish the incompressibility constraint (5), the VGT invariants become more complicated:

$$P = -A^{ii}, \tag{17}$$
$$Q = \left(P^2 - S^{ij}S^{ji} - W^{ij}W^{ji}\right)/2, \tag{18}$$
$$R = \left(-P^3 + 3PQ - S^{ij}S^{jk}S^{ki} - 3W^{ij}W^{jk}S^{ki}\right)/3, \tag{19}$$

and the phase portrait of the sysem can be represented only in three dimensions, and much more types of local behaviour

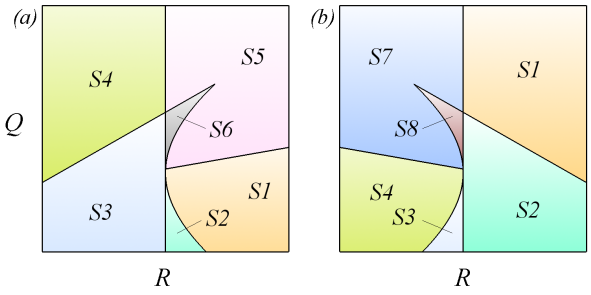

Fig. 3. $P = const.$ sections of the three dimensional phase portrait; (a) $P < 0$, (b) $P > 0$. The $P = 0$ section is identical to the plane shown in Fig. 2 for the incompressible case. Notations are described in Table I.

TABLE I
SUMMARY OF NOTATIONS IN FIG. 3 ACCORDING TO [11].

Sector	Description
S1	Unstable Focus Compressing
S2	Unstable Node/Saddle/Saddle
S3	Stable Node/Saddle/Saddle
S4	Stable Focus Stretching
S5	Stable Focus Compressing
S6	Stable Node/Stable Node/Stable Node
S7	Unstable Focus Stretching
S8	Unstable Node/Unstable Node/Unstable Node

become possible. We present these in Fig. 3 with the notations listed in Table I. As before, the discriminant of (4) separates the sectors with foci from the sectors of nodes; this yields

$$\Delta = \left(Q/3 - P^2/9\right)^3 + \left(PQ/6 - P^3/27 - R/2\right)^2 > 0 \quad (20)$$

as the *three dimensional compressible* Δ *vortex criterion* that identifies the rotation dominated behaviour as a generalisation of (15).

The relationship between the compressible three dimensional Δ and Q vortex criteria takes the form of

$$Q > P^2/3 \Rightarrow \Delta > 0, \quad \Delta < 0 \Rightarrow Q < P^2/3. \quad (21)$$

C. The VGT Equation of Motion

The equation that describes the development of the VGT can be obtained by taking the gradient of the Navier–Stokes equation [12]:

$$\frac{DA^{ij}}{Dt} + A^{ik}A^{kj} - A^{km}A^{mk}\frac{\delta^{ij}}{3} = H^{ij}, \quad (22)$$

where the first term on the LHS is the material derivative of the VGT and the matrix H^{ij} on the RHS condenses the effects of all forces acting on the fluid element. In two dimensions the number 3 in the denominator in the last term on the LHS of (22) has to be replaced by 2. For the sake of simplicity we restrain to the case of a Stokesian fluid with constant density and viscosity, then the source terms are [12]

$$H^{ij} = -\frac{1}{\rho}\left(\frac{\partial^2 p}{\partial x^i \partial x^j} - \frac{\partial^2 p}{\partial x^k \partial x^k}\cdot\frac{\delta^{ij}}{3}\right) + \nu\frac{\partial^2 A^{ij}}{\partial x^k \partial x^k}. \quad (23)$$

In general, terms due to the variability of the density and the viscosity should also appear in (23).

III. Detecting Eulerian Structures by SPH

In this section we describe an actual realization of instantaneous Eulerian flow structures in SPH, using the Δ criterion discussed in Subsection II-B.

A. SPH Details

Because in the present paper we focus on the motions and flow conditions in the interior of the fluid, for simplicity we have calculated the density directly, based only on the instantaneous configuration of particles,

$$\rho_a = \sum_b m_b W_{ab}\,, \quad (24)$$

and ignored the kernel truncation errors near the fluid boundaries. The average number of neighbours has been set to 55 particles in all calculations in this paper. For the pressure calculation the Tait equation has been used,

$$P_a = c_s^2\rho_0/\gamma\left((\rho_a/\rho_0)^\gamma - 1\right), \quad (25)$$

with the specific heat ratio $\gamma = 7$ and speed of sound $c_s = 10$. Dissipation forces have been based on the artificial viscosity model [13] with $\alpha = 0.3$. Particle positions have been updated by a second order predictor-corrector scheme.

The calculations have been carried out with our 3 dimensional SPH solver. The code has been written in C++ and the parallelization has been done in CUDA. We have performed all calculations in this paper with a 3.0 CUDA compute capability Kepler architecture GPU with 2 GiB device memory and 384 CUDA cores.

B. Generating the Velocity Gradient Tensor Field

In order to detect instantaneous Eulerian flow structures in SPH, the components and the scalar invariants of the VGT field has to be generated. The direct SPH formulation of the dynamic VGT equation (22) is not possible, because the effect of SPH forces on its RHS cannot be formulated in closed form. Therefore, the VGT has to be obtained by numerically taking the derivatives of the velocity fields.

Obviously, the roughness of the velocity field is a serious limiting factor. In order to smooth the velocity field as much as possible, we have applied the XSPH correction in the position calculation [14]

$$\frac{dr_a^i}{dt} = v_a^i + \epsilon\sum_b \frac{m_b}{\rho_{ab}}(v_b - v_a)^i W_{ab} \quad (26)$$

with $\epsilon = 0.5$, as a first step. Next, the VGT has been generated by using the standard tensor product and differentiation convention of SPH:

$$A_a^{ij} = \sum_b \frac{m_b}{\rho_b}(v_b - v_a)^i \partial^j W_{ab}. \quad (27)$$

Unfortunately, this way of calculation leads to substantial noise due to the inaccurate calculation of the derivatives. In order

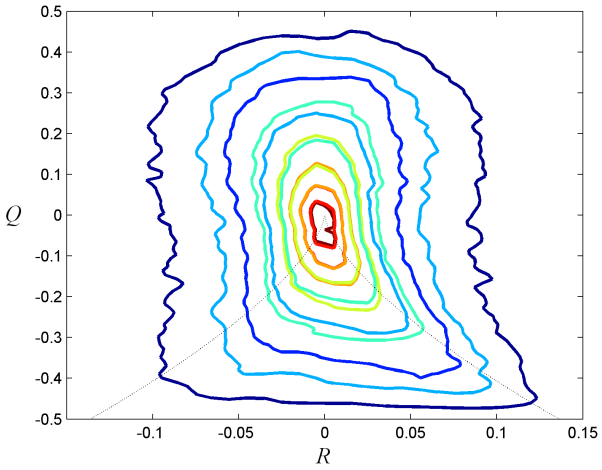

Fig. 4. PDF of particles projected to Q—R plane without correction of VGT. The $\Delta = 0$ curve is shown by dotted line. Isolines are logarithmically scaled.

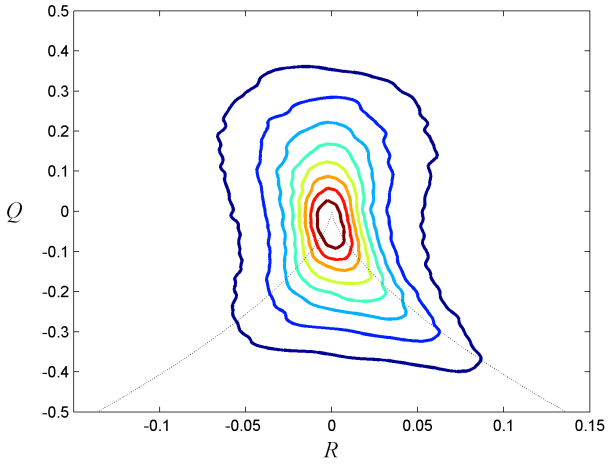

Fig. 5. PDF of particles projected to Q—R plane with correction of VGT using (28). The $\Delta = 0$ curve is shown by dotted line. Isolines are logarithmically scaled.

to achieve a smoother result, we have applied yet another correcting step similar to that of XSPH:

$$A_a^{ij} \leftarrow A_a^{ij} + \epsilon_A \sum_b \frac{m_b}{\rho_b} (A_b - A_a)^{ij} W_{ab}. \qquad (28)$$

The ϵ_A factor is left tunable (to be further discussed below).

To complete the calculation, one needs to calculate the scalar invariants from the VGT components using the formulæ in Subsection II-B. Since our fluid is weakly compressible, c.f. (25), we have had to use the three dimensional compressible forms (17–19). Finally, the Δ criterion can be evaluated using the appropriate formula (20).

The correction (28) we recommend in this procedure is a crucial step, since it produces in a substantially smoother VGT field. To study this effect, we capture the VGT components of each particle in a chosen time instant of the simulation. In order to have a comparable distribution for different cases, we normalize the VGT of each particle independently of each other using the formula

$$A_a^{ij} \leftarrow \frac{A_a^{ij}}{\sqrt{A_a^{mn} A_a^{mn}}}. \qquad (29)$$

This ensures that $-1 < A_{ij} < 1$ and that we can subsequently obtain the scalar invariants in the same compact frame without loss of information. [15]

Figures 4 and 5 show the empirical probability density functions (PDF) in the Q–R plane of the particles obtained the same calculation from the Test Case I without and with the VGT correction step, respectively. It is obvious that the distribution without correction is affected by a significant noise.

C. Test case I.

In this test, we have performed experimental calculations to study the effect of the artificial viscosity α and ϵ_A upon our correction method (28). We have simulated vortex decay in a simple vessel of cubic shape with 2 m edge size. The container was filled by a vertical jet of water until the level reached 1 m, then the inlet was closed. The instantaneous configuration of particles on Q–R plane was captured right after the incoming water had stopped.

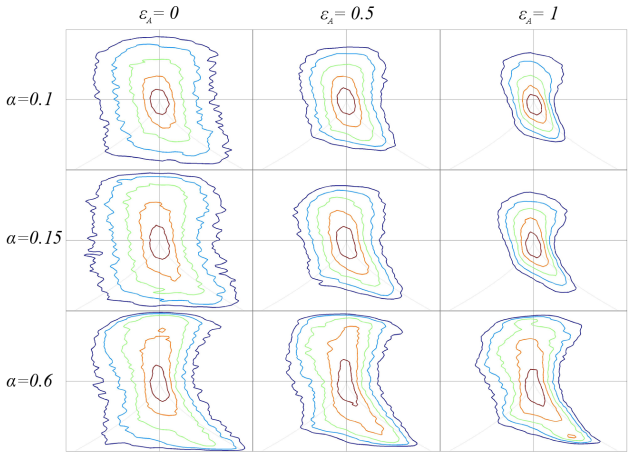

Fig. 6. Empirical probability density functions on the normalised Q—R plane obtained in case of different α and ϵ_A values in Test Case I. Isoprobability curves are logarithmically scaled.

The procedure has been repeated with several settings of α and ϵ_A. The empirically obtained distributions are presented in Fig. 6 for different cases, after using the normalization (29). The effect of α and ϵ_A on the second momentum of R in the PDF's is shown in Fig. 7, their joint smoothing effect is obvious and requires more effort to be completely understood and exploited for optimal smoothing.

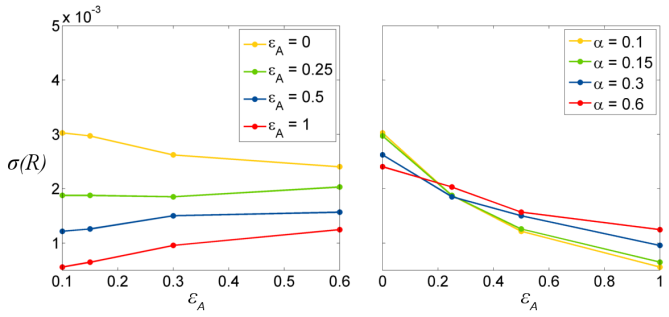

Fig. 7. The variance of R of the PDF's in Fig. 6 vs. α and ϵ_A.

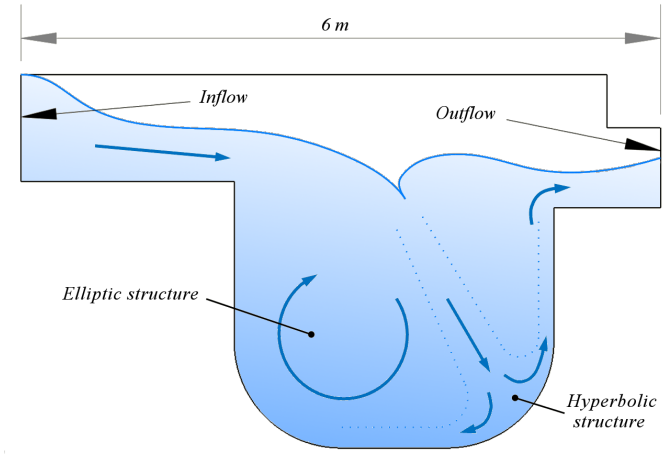

Fig. 8. Geometry of the second and third test cases.

IV. Lagrangian Flow Structure Analysis

In this section we present two simple test cases, in which we attempt to carry out simple Lagrangian flow analysis within the framework of SPH. The geometry and the flow problem is identical in both cases, it is shown in Fig. 8. The number of particles in the simulation was about $200,000$. Otherwise we used the same program settings as in the previous Section.

The first step is to use the Eulerian tools introduced in the previous Sections to identify candidates of Lagrangian flow features. We have applied the three dimensional compressible Δ and Q criteria, c.f. (20) and (21), to take this first approach. As Fig. 9 shows, by means of these criteria the rotating structures can be successfully separated from hyperbolic ones. Next we have chosen a candidate 'elliptic' and 'hyperbolic' flow feature, their location is indicated in Fig. 8, where the existence of a corresponding Lagrangian structure have been expected. Then we picked a 'core' particle inside each of these candidates, and marked the particles within close vicinity around them. In addition we have also generated *passive tracer particles* — one 'child' for each SPH marked particle — exactly at the position of its 'parent'. We realised passive tracers as special particles that are moved by the smoothed velocity field of the 'real' SPH particles, but they had no effect on the flow (nor each other).

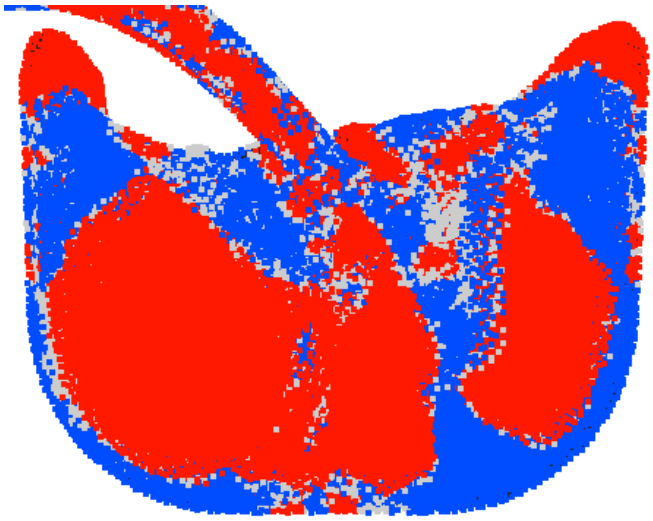

Fig. 9. Red particles indicate rotation dominated structures ($Q > 0$), blue ones signal hyperbolic flow type ($\Delta < 0$). White particles (where $Q < 0$ and $\Delta > 0$) are considered to be without dominant properties.

In the subsequent steps of the simulation we have tracked these particles and calculated their relative dispersion and finite time Lyapunov exponent (FTLE). The initially nearby particles were paired to form N couples. Their relative position dispersion was obtained by

$$D(t;t_0,d_0)^2 = \frac{1}{N/2} \sum_{a=1,3,5,\ldots} |x_a^i - x_{a+1}^i|^2, \qquad (30)$$

as defined in [6], while the FTLE was calculated as

$$\Lambda(t) = \log(d(t)/d_0)/t, \qquad (31)$$

where d_0 and $d(t)$ denote the initial and later distances between the paired particles and t is the elapsed time.

Both dispersion and FTLE have been calculated to SPH pairs, passive particle pairs and pairs of SPH and passive particles. The purpose of this investigation was to estimate the rate at which SPH particles deviate from true Lagrangian behaviour. Although we have used the XSPH correction, which causes a less erratic behaviour, it is important to calculate material trajectories as exactly as it is possible. The success of Lagrangian methods depends on how accurately the particles follow their exact material path.

A. Test Case II.

In the second test case the suspected elliptic type structure has been investigated. Fig. 10 shows the trajectories of the SPH and the passive particles side by side. For the first glance it is hard to distinguish the small differences between the two subfigures. This can be confirmed by checking out Fig. 11, which shows the relative dispersion and the FTLE time series. The dispersion between 'child'–'parent' pairs has proved to be smaller by almost two magnitudes than those among the SPH particles only or the passive tracers only. This indicates that passive tracers successfully shadow their counterparts' motion.

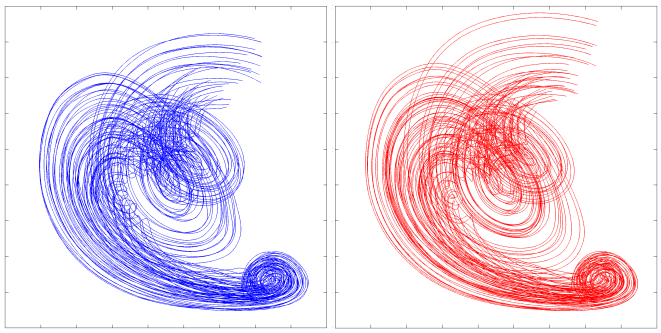

Fig. 10. The blue and red curves are the trajectories of the SPH and passive particles, respectively, in the elliptic structure of Fig. 8.

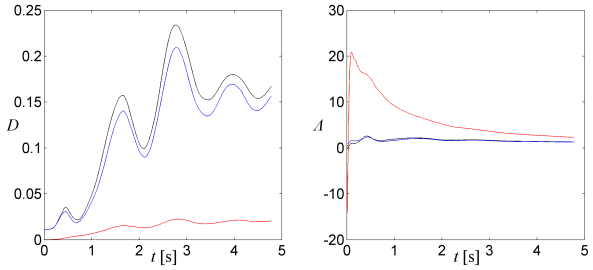

Fig. 11. Relative dispersion and FTLE in the vortical flow structure. Black, blue and red curves denote SPH, passive and mixed pairs, respectively.

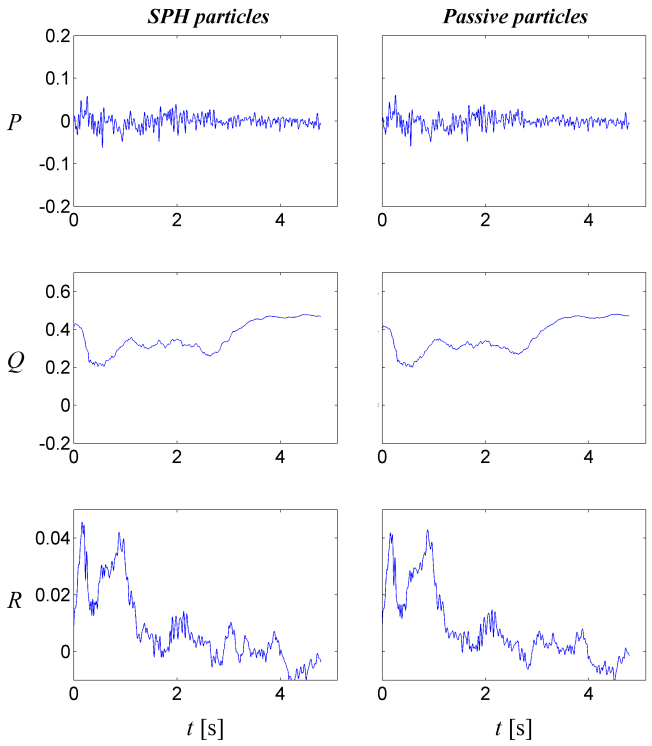

Fig. 12. Average VGT invariants of the SPH and the passive particles in the rotation dominated structure.

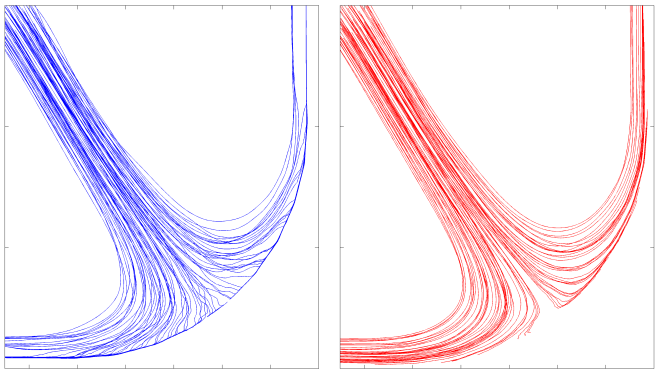

Fig. 13. Particle trajectories. Blue and red curves indicate SPH and passive particles, respectively.

The initially much larger FTLE values between mixed pairs is an artifact caused by the small initial distance between passive particles and their parent particles in (31). Fig. 12 shows the evolution of the scalar invariants of the SPH and the passive particles separately. The passive particles show very similar behaviour but with slightly less noise. The difference between the variances (not shown for clarity) was significant in favour of the passive tracers. The average values indicate that the particle cloud remained within the $Q > 0$ sectors of the Eulerian phase map, c.f. Fig. 3.

All of these findings indicate high level of coherence among these trajectories in this sample region.

B. Test Case III.

In the third test case the hyperbolic structure candidate was tested, which had been anticipated in the bottom corner of the vessel, c.f. Fig. 8. This expectation was also supported by Fig. 9. In this case the 'core' particle has been placed directly upstream of the supected hyperbolic point, right into the jet inside the fluid. The streamlines in Fig. 13 show as the group of particles and passive tracers reach the hyperbolic point on the wall where they experience flattening strain: compression in the normal direction and rapid stretching in the tangential directions. The trajectories of the tracer particles are again very similar to those of the SPH particles but they are definitely smoother. The evolution of the VGT invariants shows that reaching the hyperbolic triggers a shock-like effect especially in case of the SPH particles. The development of the passive particles again seems much smoother. The relative dispersion curve in Fig. 15 shows again an order of magnitude lower dispersion between SPH and tracer particles then among particles of the same kind. The trend of the dispersion is different from the previous test case, now the particles undergo rapid stretching right after reaching the hyperbolic point. The FTLE data shows the same artifact as before.

V. Summary

In this paper we carried out the implementation of a complete file structure analysis programme in SPH. The simulations and calculations were carried out by our three dimensional SPH solver. We argued for and implemented the compressible Δ-criterion as a potentially useful tool for

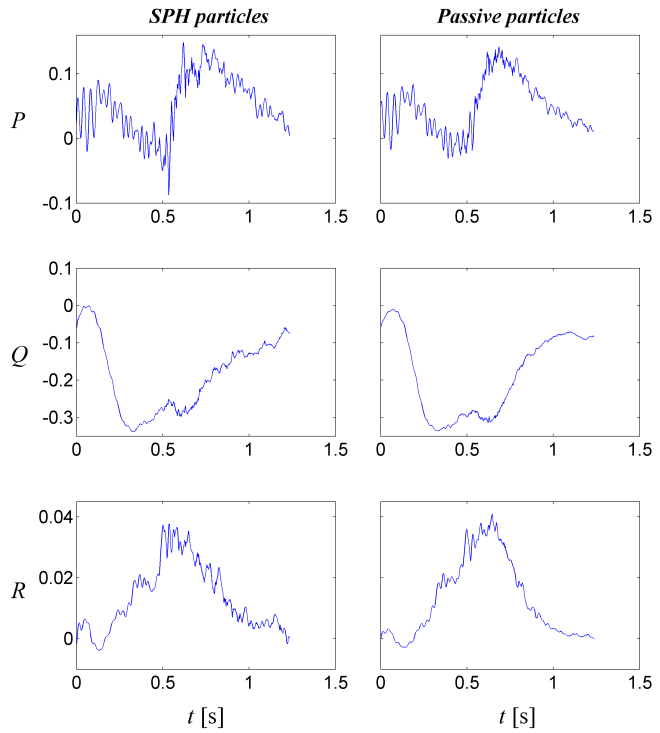

Fig. 14. Average of VGT invariants of the SPH and the passive particles around the hyperbolic point.

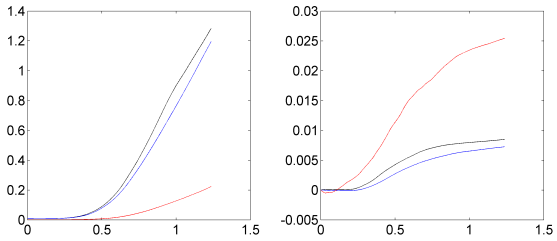

Fig. 15. Relative dispersion and FTLE in the hyperbolic flow structure. Black, blue and red curves denote SPH, passive and mixed pairs, respectively.

instantaneous Eulerian flow structures. The smoothing of the VGT field proved to be a crucial step, for which we introduced a method. The important role of a reliable instantaneous structure detection method in Lagrangian flow analysis has also been demonstrated in test cases. We have also presented information about the comforting tendency of passive tracers to shadow real SPH particles.

The analysis of the VGT invariants' distribution shows remarkable agreements with turbulent behaviour. Further work in this field may result in a more sophisticated viscosity model, which has the ability to reproduce the Kolmogorov energy cascade down to the scale of discretization. The possible adaptation to incompressible SPH which can provide simpler and more accurate methods in case of incompressible fluids. SPH carries a potential to be a succesful platform of even better and higher order Lagrangian flow analysis tools.

ACKNOWLEDGMENT

This research has been supported by the Hungarian Scientific Research Fund OTKA, grant no. K81621.

REFERENCES

[1] C. Truesdell, "Two measures of vorticity," *Journal of Rational Mechanics and Analysis*, vol. 2, pp. 173–217, 1953.

[2] G. Haller, "An objective definition of a vortex," *Journal of Fluid Mechanics*, vol. 525, pp. 1–26, 2 2005. [Online]. Available: http://journals.cambridge.org/article_S0022112004002526

[3] V. Kolář, "Compressibility effect in vortex identification," *AIAA Journal*, vol. 47, no. 2, pp. 473–475, 2009. [Online]. Available: http://arc.aiaa.org/doi/abs/10.2514/1.40131

[4] J. M. Ottino, *The kinematics of mixing: stretching, chaos, and transport*, ser. Cambridge texts in applied mathematics. Cambridge: Cambridge University Press, 1990.

[5] N. J. Zabusky, "Vortex paradigm for accelerated inhomogeneous flows: Visiometrics for the Rayleigh–Taylor and Richtmyer–Meshkov environments," *Annual Review of Fluid Mechanics*, vol. 31, pp. 495–536, 1999. [Online]. Available: http://www.annualreviews.org/doi/abs/10.1146/annurev.fluid.31.1.495

[6] A. Provenzale, "Transport by coherent barotropic vortices," *Annual Review of Fluid Mechanics*, vol. 31, pp. 55–93, 1999. [Online]. Available: http://www.annualreviews.org/doi/abs/10.1146/annurev.fluid.31.1.55

[7] G. Haller and F. J. Beron-Vera, "Coherent Lagrangian vortices: the black holes of turbulence," *Journal of Fluid Mechanics*, vol. 731, 9 2013. [Online]. Available: http://journals.cambridge.org/article_S0022112013003911

[8] J. Weiss, "The dynamics of enstrophy transfer in two-dimensional hydrodynamics," *Physica D: Nonlinear Phenomena*, vol. 48, no. 2-3, pp. 273–294, 1991. [Online]. Available: http://www.sciencedirect.com/science/article/B6TVK-46JYG9X-CP/2/2cb2d00cb92d6305fc992f6689c7cf9f

[9] A. Okubo, "Horizontal dispersion of floatable particles in the vicinity of velocity singularities such as convergences," *Deep Sea Research and Oceanographic Abstracts*, vol. 17, no. 3, pp. 445–454, 1970. [Online]. Available: http://www.sciencedirect.com/science/article/B757H-48CG2TJ-12V/2/81594a2913c0607cd1a64743959e4e8c

[10] H. M. Blackburn, N. N. Mansour, and B. J. Cantwell, "Topology of fine-scale motions in turbulent channel flow," *Journal of Fluid Mechanics*, vol. 310, pp. 269–292, 3 1996. [Online]. Available: http://journals.cambridge.org/article_S0022112096001802

[11] Y.-B. Chu and X.-Y. Lu, "Topological evolution in compressible turbulent boundary layers," *Journal of Fluid Mechanics*, vol. 733, pp. 414–438, 10 2013. [Online]. Available: http://journals.cambridge.org/article_S0022112013003996

[12] B. J. Cantwell, "Exact solution of a restricted Euler equation for the velocity gradient tensor," *Physics of Fluids A: Fluid Dynamics*, vol. 4, no. 4, pp. 782–793, 4 1992.

[13] J. J. Monaghan and R. A. Gingold, "Shock Simulation by the particle method SPH," *Journal of Computational Physics*, vol. 52, no. 2, pp. 374–389, 1983.

[14] J. J. Monaghan, "On the problem of penetration in particle methods," *Journal of Computational Physics*, vol. 82, no. 1, pp. 1–15, May 1989. [Online]. Available: http://dx.doi.org/10.1016/0021-9991(89)90032-6

[15] S. Suman and S. S. Girimaji, "Homogenized Euler equation: a model for compressible velocity gradient dynamics," *Journal of Fluid Mechanics*, vol. 620, pp. 177–194, 2 2009. [Online]. Available: http://journals.cambridge.org/article_S0022112008004631